

Temperature dependence of charge conversion during NV-center relaxometry

Isabel Cardoso Barbosa, Jonas Gutsche, Dennis Lönard, Stefan Dix, and Artur Widera*
*Department of Physics and State Research Center OPTIMAS,
University of Kaiserslautern-Landau,
Erwin-Schroedinger-Str. 46, 67663 Kaiserslautern, Germany*

(Dated: September 22, 2023)

Temperature-dependent nitrogen-vacancy (NV)-center relaxometry is an established tool to characterize paramagnetic molecules near to a sensing diamond, gaining momentum in different fields of science. However, recent results indicate that conversion between NV-center charge states impedes these measurements and influences the results for the T_1 time. While the temperature dependence of NV centers' T_1 time is well-studied, additional contributions from temperature-dependent charge conversion during the dark time may further affect the measurement results. We combine temperature-dependent relaxometry and fluorescence spectroscopy at varying laser powers to unravel the temperature dependence of charge conversion in nanodiamond for biologically relevant temperatures. While we observe a decrease of the T_1 time with increasing temperatures, charge conversion remains unaffected by the temperature change. These results allow the temperature-dependent performance of T_1 relaxometry without further consideration of temperature dependence of charge conversion.

I. INTRODUCTION

The negatively charged NV center in diamond is an established tool for spatially-resolved mapping of temperatures [1], magnetic fields [2], and electric fields [3] as so-called quantum sensors [4]. Because of their small sizes, nanodiamonds provide an advantageous NV host for different fields of science. Nanodiamonds can be brought into cells or organelles [5–7] and trace chemical reactions via NV-center relaxometry [8, 9], which is the measurement of the NV centers' longitudinal spin-relaxation time T_1 [10]. In a chemical reaction, not only the formation of a paramagnetic product, but also changes in the temperature or the pH may contribute to a T_1 change [9]. Moreover, recent studies indicate that another mechanism challenges T_1 relaxometry: the illumination-induced charge conversion between NV-charge states during a pulsed-laser measurement [11–13]. These ionization processes between the negatively charged NV^- and the neutrally charged NV^0 impact the NV^- fluorescence recorded during the T_1 measurement. With temperatures potentially increasing during reactions, the question arises whether an additional contribution due to temperature-dependent charge conversion must be considered when interpreting changes in the relaxometry signal.

In our work, we perform NV fluorescence spectroscopy to derive ratios of NV^- and NV^0 and compare them for different temperatures. We perform relaxometry at different laser powers to derive the longitudinal spin-relaxation times for an NV ensemble in nanodiamond and the recharge times from NV^0 to NV^- in the

dark for biologically-relevant temperatures [9, 14] from 20 °C to 75 °C (294 K to 348 K). The combination of these two techniques allows us to trace the ratio $[NV^-]/[NV^0]$ during the relaxometry sequence as a function of the temperature.

We non-resonantly excite the negatively charged NV center ensemble in our sample with a 520 nm laser from their triplet ground state to their triplet excited state [4, 15]. Due to the spin-state dependent transition rates between the NV^- states [16, 17], spin polarization toward the $m_S = 0$ state is achieved [10]. This spin polarization relaxes over the typical time scale T_1 until the population decays to a thermally mixed state [10]. During laser illumination, ionization from NV^- to NV^0 can take place [18–21], and recharging from NV^0 to NV^- in the dark then contributes to the measured NV^- fluorescence signal [11–13]. While common T_1 measurement schemes include a microwave- π pulse between laser pulses to mitigate influences from background fluorescence [22, 23], the microwave pulse is often omitted in biological applications to avoid undesired heating of samples [6–8]. Therefore, these all-optical T_1 measurements are susceptible to influences from charge conversion. With the temperatures potentially rising during chemical reactions, the NV^- fluorescence signal could be influenced by T_1 's temperature dependence [22–24] and charge conversion changing with increasing temperature.

II. METHODS

We excite ensembles of NV centers in a single nanodiamond of size ~ 750 nm (Adamas Nano, NDNV/NVN700nm2mg) with a 520 nm laser and collect their fluorescence. According to the manufacturer, the nanodiamonds contain ~ 0.5 ppm of NV centers and

* Author to whom correspondence should be addressed: widera@physik.uni-kl.de

~ 37 ppm of substitutional nitrogen. The laser beam is focused to a spot size of ~ 700 nm ($1/e^2$ diameter) with a maximum laser power of 4 mW, and we adjust lower laser powers with an acousto-optic modulator (AOM). We simultaneously record fluorescence spectra of NV^- and NV^0 in the range between 550 nm and 775 nm. Moreover, we decompose and analyze the fluorescence spectra according to Ref. [25], allowing us to calculate fractions of $[\text{NV}^-]$ and ratios of $[\text{NV}^-]/[\text{NV}^0]$ at specific laser powers and temperatures. Additional details on the spectral analysis in this work are given in Appendix A. We perform a common relaxometry sequence for NV-center relaxometry, including 520 nm-laser pulses generated with an AOM and a microwave- π pulse.

To detect the fluorescence of NV^- and NV^0 separately in two single-photon-counting modules (SPCMs), we split the fluorescence and equip the beam paths with a 665 nm longpass filter (NV^- fluorescence) and a 600 nm shortpass filter (NV^0 fluorescence). Details on the experimental setup and the pulsed sequence are described in [13]. Using the described method in [13], we map the NV-charge-state ratio obtained from fluorescence spectroscopy to count-rate ratios in the SPCMs. This mapping allows us to trace the ratio $[\text{NV}^-]/[\text{NV}^0]$ during the relaxometry sequence and get an insight into charge conversion within the relaxation time. In this analysis, we correct fluorescence counts for the wavelength-dependent absorption of neutral density filters we employ to keep the SPCMs below saturation. Additionally, we consider dark counts recorded with each SPCM. Microwave signals are generated, amplified, and brought close to the nanodiamond with a microwave antenna which is similar to the design described in Ref. [26]. We employ a temperature-controlled sample holder to perform temperature-dependent fluorescence spectroscopy and relaxometry. Built-in Peltier elements are used to heat the sample and keep the temperature constant at temperatures between room temperature and ~ 350 K. We derive the temperature at the nanodiamond location via optically-detected magnetic resonance (ODMR) spectroscopy employing the temperature dependence of the NVs' zero-field splitting (ZFS) of (-74.2 ± 0.7) kHz K^{-1} [27]. We perform all experiments in a magnetic bias field in the order of 8 mT to split the NV centers' spin resonances and avoid cross relaxations [22].

III. RESULTS AND DISCUSSION

A. Temperature-dependent spectra decomposition

The decomposed fluorescence spectra of NV^- and NV^0 are shown in Fig. 1 for temperatures of 294 K and 348 K. We observe an increase in the NV^- and NV^0 zero-phonon line (ZPL) widths and a shift of their posi-

tions to higher wavelengths caused by the temperature increase as previously described by [28–32], see also Appendix B. The fractional concentration of NV^- with respect to the sum of $[\text{NV}^-]$ and $[\text{NV}^0]$ is derived by the fractional contributions c_- and c_0 of NV^- and NV^0 to the composed fluorescence spectrum with

$$\frac{[\text{NV}^-]}{[\text{NV}^-] + [\text{NV}^0]} = \frac{c_-}{c_- + \kappa_{520}c_0}, \quad (1)$$

where $c_- + c_0 = 1$, and κ_λ (here, $\lambda = 520$ nm) is a correction factor that describes the photoluminescence ratios of NV^- and NV^0 [25]. In the spectral analysis, we calculate κ_{520} similarly as described in Ref. [25] and our previous work [13]. For this, we record fluorescence spectra at laser powers well below saturation [33] and correct them for the exposure times they were recorded with. We decompose the spectra into contributions from NV^- and NV^0 and calculate fluorescence intensities for NV^- and NV^0 for each laser power. We fit the fluorescence intensities of NV^- and NV^0 as a function of the laser power in a weighted linear fit and directly compare the slopes of the integrated fluorescence intensities of NV^- and NV^0 . By forming the quotient of these slopes, we obtain κ_{520} .

We perform this spectral analysis for different temperatures ranging from 294 K to 348 K. The values obtained for κ_{520} show a relatively constant value around $\kappa_{520} \sim 1.65$, see Fig. 2. The error of the temperatures is derived from the fit error of the resonances measured

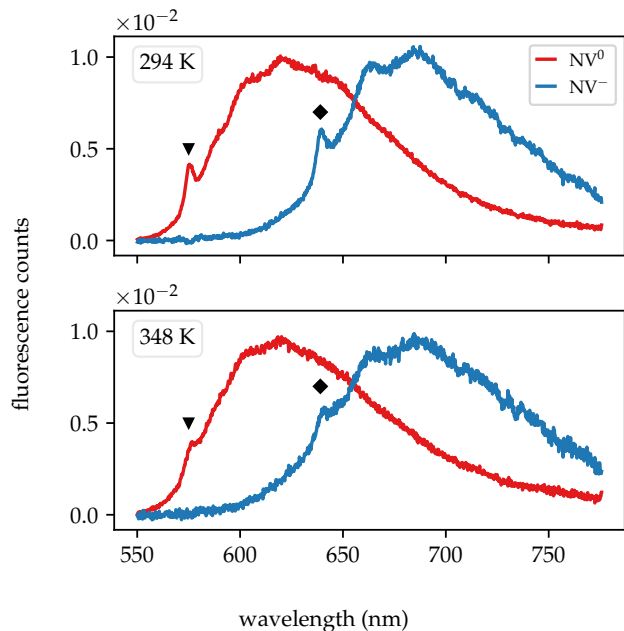


FIG. 1. Decomposed fluorescence spectra for NV^- and NV^0 for temperatures of 294 K and 348 K. The ZPLs of NV^- and NV^0 at 575 nm (\blacktriangledown) and 639 nm (\blacklozenge), respectively, are broadened and shifted to higher wavelengths at 348 K compared to 294 K.

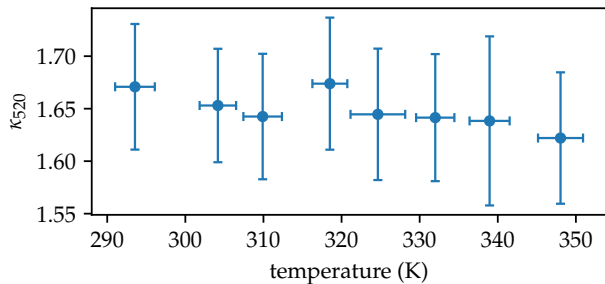


FIG. 2. Calculated κ_{520} as a function of the temperature. We derive κ_{520} from spectral analysis at each temperature as described in the main text.

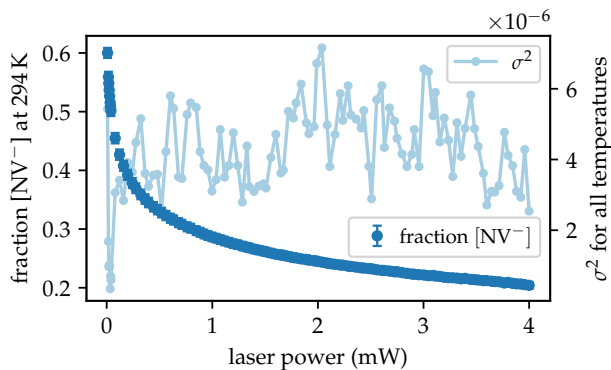


FIG. 3. Calculated fraction of $[\text{NV}^-]$ as a function of the laser power at 294 K. Representing increased temperatures up to 348 K, the variance σ^2 between the $[\text{NV}^-]$ fractions at each temperature is shown as a function of the laser power.

with ODMR spectroscopy and the uncertainty of the temperature dependence of the NVs' ZFS [27]. We derive the standard error for κ_{520} from linear fitting of the fluorescence intensities we obtain for NV^- and NV^0 , weighted with the statistical error of the intensities we obtain in the spectral analysis (inverse-variance fit).

Additionally, we record NV fluorescence spectra for laser powers up to 4 mW at each temperature. Using the values for κ_{520} we obtain for each temperature and the decomposed spectra, we calculate the fractional concentration of NV^- according to Eq. (1) for each laser power and temperature. We obtain the error for the $[\text{NV}^-]$ fraction from the errors for κ_{520} , c_- , and c_0 . The result for the $[\text{NV}^-]$ fraction as a function of the laser power is shown in Fig. 3 for 294 K. At very low laser powers of $\sim 8 \mu\text{W}$, the fraction of $[\text{NV}^-]$ is above 60%, while it decreases to 20% at high laser powers of $\sim 4 \text{ mW}$. Although the fluorescence spectra in Fig. 1 change visibly with increasing temperature, the fractions of $[\text{NV}^-]$ qualitatively show the same behavior as a function of the laser power for all temperatures. To point out differences between temperatures in more detail, we show the variance σ^2 of the

$[\text{NV}^-]$ fractions between all eight temperatures for all laser powers in Fig. 3. With σ^2 staying in the order of 10^{-6} for all laser powers, we confirm that the NV^- fraction as a function of the laser power does not depend on the temperature in our sample.

B. Temperature-dependent relaxometry

To get an insight into the temperature dependence of the T_1 spin-relaxation time and charge conversion in our sample, we perform T_1 relaxometry using a common sequence shown in Fig. 4 (a) [22, 23] at different temperatures and laser powers. A laser pulse of 200 μs spin polarizes the NV^- centers to their $m_S = 0$ states. After 1 μs , a 5 μs laser pulse probes the fluorescence intensity before the variable relaxation time τ for normalization. The π pulse performed during τ acts upon NV^- centers of a specific orientation in the diamond lattice and excites their population from $m_S = 0$ to $m_S = +1$ or $m_S = -1$ of the electronic ground state. Another 5 μs laser pulse reads out the fluorescence intensity after τ in the signal detection windows. Between readout and subsequent spin polarization, a pause time t_p of 1 ms is inserted to mitigate build-up effects during the cycle. Each cycle is repeated 50 000 times and the complete sequence is swept multiple times. By subtraction of the NV^- fluorescence in the signal detection windows, we obtain a difference in fluorescence between $m_S = 0$ and $m_S = +1$ or $m_S = -1$ states as a measure of the spin polarization of the NV^- centers excited by the π pulse [22, 23]. Using the second half of the sequence, we obtain a normalized fluorescence of NV^- by division of the signal fluorescence counts by the normalization fluorescence counts for all NV-center orientations. This analysis corresponds to an all-optical T_1 measurement scheme as often employed in biology [6, 7, 9]. We conduct the sequence with low laser powers of $\sim 8 \mu\text{W}$ to prevent charge conversion from prevailing. We fit both decays we obtain from the two evaluation methods, with and without the π pulse, with a monoexponential function for each temperature to derive the T_1 time for NV^- . The results are shown as $1/T_1$ in Fig. 4 (b). We derive the error for $1/T_1$ for each temperature from the standard error of T_1 we obtain from the exponential fit. Within the ranges of their fit errors, $1/T_1$ is equal for both evaluation methods at each temperature. This result concludes that NV^- spin relaxation is dominant due to the low laser power applied, and charge conversion is negligible. Additionally, we observe an increase of $1/T_1$ with the temperature.

The temperature dependence of $1/T_1$ over a wide temperature range has previously been investigated in Refs. [22, 23] for NV centers in bulk samples of different defect concentrations and further described in [24]. It was found in Refs. [22, 23] that the observed behavior can be assigned to two-phonon Raman and Orbach-type

processes, and the data fit according to

$$\frac{1}{T_1} = A_1(S) + \frac{A_2}{e^{\Delta/kT} - 1} + A_3 T^5. \quad (2)$$

Here, only the parameter $A_1(S)$ depends on the sample, while A_2 , A_3 , and Δ are universal parameters [22, 23]. Moreover, recent studies link the temperature dependence of the NV centers' photoluminescence intensity and spin contrast to similar electron-phonon interactions [34]. We take the values for A_2 , A_3 , and Δ as given in [22] and fit the function to our measurement data sets. The resulting function with a mean parameter of A_1 from the signals with and without the π pulse can be seen as a red solid line in Fig. 4 (b). Qualitatively, this fit models our data well. We find $A_1 = (657 \pm 13) \text{ s}^{-1}$, which generally lies within the orders of magnitude given in Refs. [22, 23]. We note that the value for A_1 found for our nanodiamond sample is higher compared to A_1 found in a bulk diamond of comparable NV-center concentration [22, 23]. Possible reasons for this discrepancy may be the different alignment of the external magnetic field relative to the NV-center axes in our experiments or a different concentration of substitutional nitrogen atoms in our sample. Additionally, recent studies show that the high-temperature annealing of our sample affects on the NV centers' T_1 time [35], which could also result in a different A_1 compared to the samples in Refs. [22, 23].

To enhance and trace charge conversion during relaxometry, we perform the same sequence in Fig. 4 (a) with a higher laser power of 0.56 mW, omit the microwave π pulse, and collect the NV^- and NV^0 fluorescence in two separate detectors. At high laser powers, NV^- is converted to NV^0 during the spin polarization pulse [12, 18]. During the relaxation time τ , recharge occurs from NV^0 to NV^- , causing the NV^0 fluorescence to decay over τ , while the NV^- fluorescence increases [12, 13]. We interpret this decay of the NV^0 fluorescence in the dark as the recharging time of NV^0 to NV^- [11]. In our nanodiamond sample, the decay of the normalized NV^0 fluorescence cannot be sufficiently described with a monoexponential function [13]. Therefore, we fit a biexponential function to the normalized NV^0 fluorescence as a function of τ to obtain the characteristic recharge times $T_{R,1}$ and $T_{R,2}$ for our sample. The result is shown in Fig. 5 as $1/T_{R,1}$ and $1/T_{R,2}$. We calculate the errors for $1/T_{R,1}$ and $1/T_{R,2}$ from the standard errors we obtain for $T_{R,1}$ and $T_{R,2}$ in the biexponential fit. It can be clearly seen in Fig. 5 that $1/T_{R,1}$ and $1/T_{R,2}$ are constant as a function of the temperature. From this, we conclude that the charge dynamics in our pulsed measurement are independent of the temperature in the observed range. In our previous work, several nanodiamonds were investigated with the same measurement scheme and a similar biexponential decay of the NV^0 fluorescence was observed [13]. Therefore, we expect other nanodiamonds of the same kind to exhibit an analogous behavior with

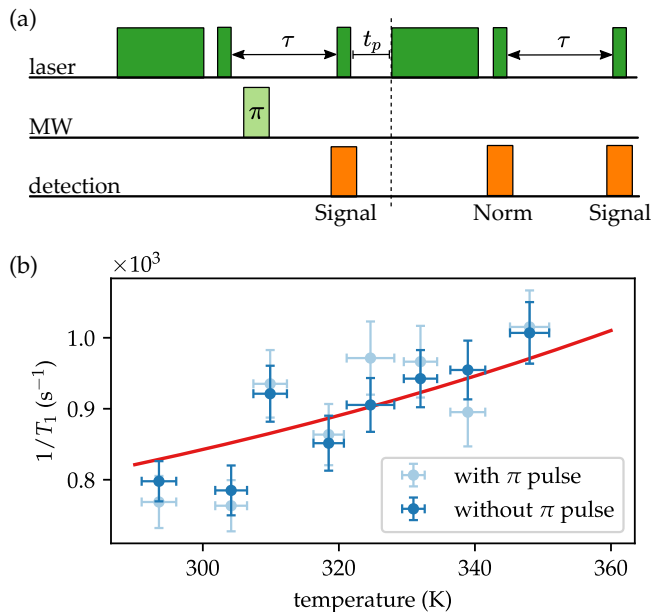


FIG. 4. NV-center relaxometry scheme and result for $1/T_1$ as a function of the temperature. (a) The pulsed scheme uses laser spin-polarization and readout pulses. Additionally, we apply a microwave π pulse in the first half of the sequence. The T_1 time, accessed with the π pulse, is obtained by forming the difference of the fluorescence counts in the two signal detection windows and fitting a monoexponential function to the result. Further, with the same measurement, we recover the all-optical T_1 time in the second half by dividing the fluorescence counts in the signal detection window by the fluorescence counts in the normalization detection window and fitting a monoexponential function to the result. (b) Result for $1/T_1$ for each temperature, evaluated with the π pulse applied and without. The red solid line is a fit as explained in the main text.

increasing temperature.

The suggested mechanism for the NV^- to NV^0 charge-conversion process is tunneling, mediated by substitutional nitrogen atoms in the diamond lattice [20, 36]. This effect depends on the nitrogen concentration in diamond [18, 36], and is not influenced by an increase of the temperature in our sample. The temperature dependence on NV-center charge conversion has previously been investigated for temperatures below room temperature [37, 38]. While charge conversion did not show any temperature dependence in [38], an exponential increase of the $[\text{NV}^-]/[\text{NV}^0]$ ratio with decreasing temperature was found in a different sample in [37]. Since we examine the temperature dependence of charge conversion above room temperature, our findings conform with both observations mentioned above. To get an insight into the temperature dependence of charge conversion in our sample below room temperature, measurements at cryogenic temperatures will have to be performed.

To examine the effect of increasing temperature on

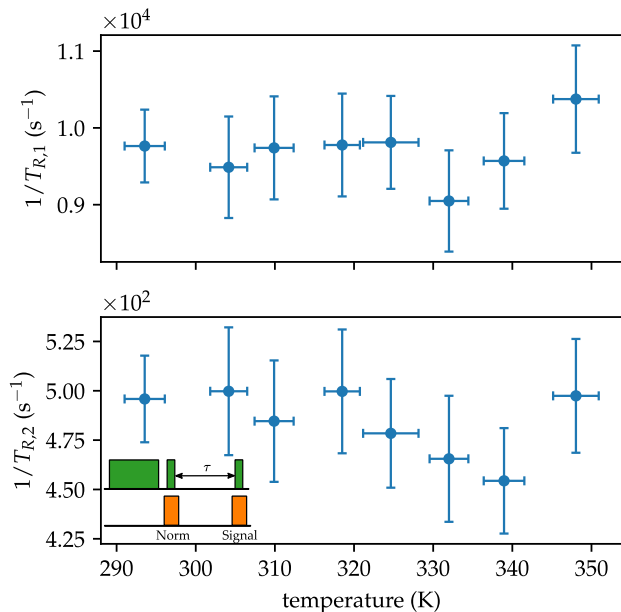


FIG. 5. Derived values of $1/T_{R,1}$ and $1/T_{R,2}$ as a function of the temperature. We obtain the recharge rates from a biexponential fit to the normalized NV^0 fluorescence, recorded with the relaxometry sequence (π pulse omitted) at 0.56 mW laser power. The inset displays the characteristics of the pulsed sequence applied.

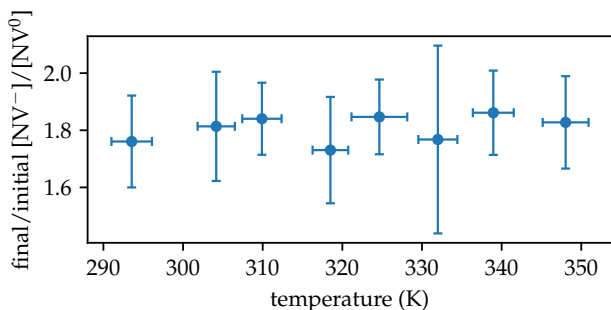


FIG. 6. Charge-state ratio of $[NV^-]$ to $[NV^0]$ at the longest τ divided by the ratio at the shortest τ as a function of the temperature. The data is derived from spectral analysis and relaxometry recorded with 0.56 mW laser power.

charge dynamics, we trace the ratio $[NV^-]/[NV^0]$ during the relaxometry measurement at different temperatures. For this, we use the results from the spectral analysis to derive $[NV^-]/[NV^0]$ during the relaxometry sequence in the signal detection window in the second half of the relaxometry measurement scheme. This way, we gain insight into the charge dynamics during the relaxation time τ . Conform with the decrease of the NV^0 fluorescence during τ , we observe an increase of the ratio $[NV^-]/[NV^0]$. We plot the ratio $[NV^-]/[NV^0]$ at the last τ divided by the ratio $[NV^-]/[NV^0]$ at the first τ

for 0.56 mW laser power as a function of the temperature in Fig. 6. We calculate the errors in Fig. 6 from the standard fit errors we obtain from mapping the ratio of $[NV^-]/[NV^0]$ to count rate ratios in a fit of form $ax^n + c$ for each temperature. The fit is weighted with the errors for the ratio of $[NV^-]/[NV^0]$ we obtain from the spectral analysis and the standard deviation of the count rates we measure in the SPCMs. As shown in Fig. 6, the increase of the ratio $[NV^-]/[NV^0]$ within the full measurement sequence is around 1.8, and constant with the temperature for a laser power of 0.56 mW. Similarly, for a lower laser power of 8 μ W, we observe that the increase of the ratio $[NV^-]/[NV^0]$ during τ is independent of the temperature. The temperature increase does not affect the charge dynamics during the relaxometry sequence in our sample.

IV. CONCLUSIONS

We conduct temperature-dependent fluorescence spectroscopy and relaxometry of an NV-center ensemble in nanodiamond. With this, we examine the temperature dependence of charge conversion between NV^- and NV^0 in a biologically relevant temperature range from 294 K to 350 K. We perform fluorescence-spectra decomposition at different temperatures and find that κ_{520} , which describes the photoluminescence ratio between NV^- and NV^0 , is temperature-independent. Derived from fluorescence-spectra analysis, we observe that the NV^- fraction decreases with increasing laser power but is not susceptible to the temperature. While we notice a temperature dependence of $1/T_1$ in our sample, the recharge rates $1/T_{R,1}$ and $1/T_{R,2}$ in the dark are not influenced by the temperature increase. Therefore, an additional factor in temperature-dependent relaxometry caused by charge conversion between NV-charge states does not need to be considered in applied temperature-dependent nanodiamond relaxometry. Since the substitutional nitrogen concentration influences the charge-conversion process, systematic studies of diamonds of different nitrogen concentrations will give us further insight into the mechanism of this process. Expanding the temperature range from the biologically relevant region to cryogenic temperatures will unravel the temperature dependence in more detail, allowing us to obtain fundamental knowledge about charge conversion.

ACKNOWLEDGMENTS

We acknowledge support from the nanostructuring center (NSC) of the RPTU Kaiserslautern-Landau. This project was funded by the Deutsche Forschungsgemeinschaft (DFG, German Research Foundation)—Project-ID No. 454931666. Further, I. C. B. thanks the Studiens-

tiftung des deutschen Volkes for financial support. We thank O. Opaluch and E. Neu-Ruffing for providing the microwave antenna in our experimental setup. Furthermore, we thank S. Barbosa for fruitful discussions and experimental support.

Appendix A: Spectral analysis

Before our spectral analysis, we corrected the fluorescence spectra for wavelength-dependent properties of optical elements in our beam path. Additionally, we subtract a background from each fluorescence spectrum. We decompose the fluorescence spectra into basis functions of NV^- and NV^0 according to Ref. [25] and follow their nomenclature. As described in Ref. [25], an area-normalized spectrum $\hat{I}_0^{\text{pre}}(\lambda)$, that we recorded with 4 mW laser power, and an area-normalized spectrum $\hat{I}_-^{\text{pre}}(\lambda)$, that we recorded with 8 μ W laser power, are employed to construct the basis function for NV^- with

$$I_-(\lambda) = \hat{I}_-^{\text{pre}}(\lambda) - \delta_0 \hat{I}_0^{\text{pre}}(\lambda). \quad (\text{A1})$$

For unambiguous data evaluation, we optimize δ_0 for all temperatures separately and use their mean as a constant δ_0 for all temperatures. Further, as described in Ref. [25], the NV^- basis function is area-normalized to $\hat{I}_-(\lambda)$ and the basis function for NV^0 calculated with

$$I_0(\lambda) = \hat{I}_0^{\text{pre}}(\lambda) - \delta_- \hat{I}_-(\lambda). \quad (\text{A2})$$

The value for δ_- is kept constant throughout our analysis presented in this paper.

In our previous work in Ref. [13], we investigated several nanodiamonds of similar composition. We performed the spectral analysis described in Ref. [25] to obtain NV^- fractions as a function of the laser power. We verified that our results are fundamentally equal for all examined nanodiamonds.

Appendix B: Temperature-dependent spectroscopy

For better visualization, we plot the ZPL regions of the decomposed spectra of NV^- and NV^0 for different temperatures in Fig. 7. For NV^- and NV^0 , we observe an increase in the ZPL width and a shift to higher wavelengths with increasing temperatures.

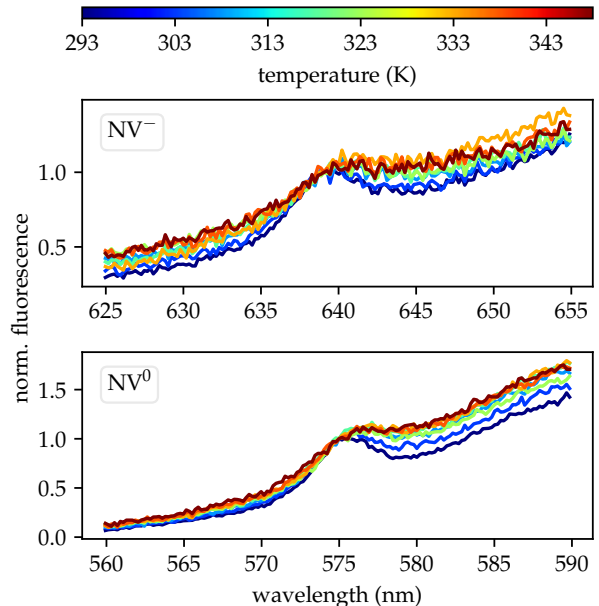


FIG. 7. ZPL regions of the decomposed spectra of NV^- and NV^0 , normalized to the spectrum intensity at 639 nm and 575 nm, respectively, for different temperatures.

-
- [1] G. Kucsko, P. C. Maurer, N. Y. Yao, M. Kubo, H. J. Noh, P. K. Lo, H. Park, and M. D. Lukin, Nanometre-scale thermometry in a living cell, *Nature* **500**, 54 (2013).
 - [2] L. Rondin, J.-P. Tetienne, T. Hingant, J.-F. Roch, P. Maletinsky, and V. Jacques, Magnetometry with nitrogen-vacancy defects in diamond, *Rep. Prog. Phys.* **77**, 056503 (2014).
 - [3] F. Dolde, H. Fedder, M. W. Doherty, T. Nöbauer, F. Rempp, G. Balasubramanian, T. Wolf, F. Reinhard, L. C. L. Hollenberg, F. Jelezko, and J. Wrachtrup, Electric-field sensing using single diamond spins, *Nat. Phys.* **7**, 459 (2011).
 - [4] J. F. Barry, J. M. Schloss, E. Bauch, M. J. Turner, C. A. Hart, L. M. Pham, and R. L. Walsworth, Sensitivity optimization for NV-diamond magnetometry, *Rev. Mod. Phys.* **92**, 015004 (2020).
 - [5] R. Sharmin, T. Hamoh, A. Sigaeva, A. Mzyk, V. G. Damle, A. Morita, T. Vedelaar, and R. Schirhagl, Fluorescent Nanodiamonds for Detecting Free-Radical Generation in Real Time during Shear Stress in Human Umbilical Vein Endothelial Cells, *ACS Sens.* **6**, 4349 (2021).
 - [6] A. Sigaeva, H. Shirzad, F. P. Martinez, A. C. Nusantara, N. Mougios, M. Chipaux, and R. Schirhagl, Diamond-Based Nanoscale Quantum Relaxometry for Sensing Free Radical Production in Cells, *Small* **18**, 2105750 (2022).
 - [7] A. Mzyk, A. Sigaeva, and R. Schirhagl, Relaxometry with Nitrogen Vacancy (NV) Centers in Diamond, *Acc. Chem. Res.* **55**, 3572 (2022).
 - [8] J. Barton, M. Gulka, J. Tarabek, Y. Mindarava, Z. Wang, J. Schimer, H. Raabova, J. Bednar, M. B. Plenio, F. Jelezko, M. Nesladek, and P. Cigler, Nanoscale Dynamic Readout of a Chemical Redox Process Using Radicals Coupled

- with Nitrogen-Vacancy Centers in Nanodiamonds, *ACS Nano* **14**, 12938 (2020).
- [9] L. Nie, A. C. Nusantara, V. G. Damle, R. Sharmin, E. P. P. Evans, S. R. Hemelaar, K. J. van der Laan, R. Li, F. P. Perona Martinez, T. Vedelaar, M. Chipaux, and R. Schirhagl, Quantum monitoring of cellular metabolic activities in single mitochondria, *Sci. Adv.* **7**, eabf0573 (2021).
- [10] E. V. Levine, M. J. Turner, P. Kehayias, C. A. Hart, N. Langellier, R. Trubko, D. R. Glenn, R. R. Fu, and R. L. Walsworth, Principles and techniques of the quantum diamond microscope, *Nanophotonics* **8**, 1945 (2019).
- [11] R. Giri, F. Gorrini, C. Dorigoni, C. E. Avalos, M. Cazzanelli, S. Tambalo, and A. Bifone, Coupled charge and spin dynamics in high-density ensembles of nitrogen-vacancy centers in diamond, *Phys. Rev. B* **98**, 045401 (2018).
- [12] R. Giri, C. Dorigoni, S. Tambalo, F. Gorrini, and A. Bifone, Selective measurement of charge dynamics in an ensemble of nitrogen-vacancy centers in nanodiamond and bulk diamond, *Phys. Rev. B* **99**, 155426 (2019).
- [13] I. Cardoso Barbosa, J. Gutsche, and A. Widera, Impact of charge conversion on NV-center relaxometry, *Phys. Rev. B* **108**, 075411 (2023).
- [14] D. Chrétien, P. Bénit, H.-H. Ha, S. Keipert, R. El-Khoury, Y.-T. Chang, M. Jastroch, H. T. Jacobs, P. Rustin, and M. Rak, Mitochondria are physiologically maintained at close to 50 °C, *PLoS Biol.* **16**, e2003992 (2018).
- [15] M. W. Doherty, N. B. Manson, P. Delaney, and L. C. L. Hollenberg, The negatively charged nitrogen-vacancy centre in diamond: the electronic solution, *New J. Phys.* **13**, 025019 (2011).
- [16] L. Robledo, H. Bernien, T. van der Sar, and R. Hanson, Spin dynamics in the optical cycle of single nitrogen-vacancy centres in diamond, *New J. Phys.* **13**, 025013 (2011).
- [17] J.-P. Tetienne, L. Rondin, P. Spinicelli, M. Chipaux, T. Debuisschert, J.-F. Roch, and V. Jacques, Magnetic-field-dependent photodynamics of single NV defects in diamond: an application to qualitative all-optical magnetic imaging, *New J. Phys.* **14**, 103033 (2012).
- [18] N. B. Manson and J. P. Harrison, Photo-ionization of the nitrogen-vacancy center in diamond, *Diam. Relat. Mater.* **14**, 1705 (2005).
- [19] N. Aslam, G. Waldherr, P. Neumann, F. Jelezko, and J. Wrachtrup, Photo-induced ionization dynamics of the nitrogen vacancy defect in diamond investigated by single-shot charge state detection, *New J. Phys.* **15**, 013064 (2013).
- [20] N. B. Manson, M. Hedges, M. S. J. Barson, R. Ahlefeldt, M. W. Doherty, H. Abe, T. Ohshima, and M. J. Sellars, NV – $-N +$ pair centre in 1b diamond, *New J. Phys.* **20**, 113037 (2018).
- [21] S. Dhomkar, H. Jayakumar, P. R. Zangara, and C. A. Meriles, Charge Dynamics in near-Surface, Variable-Density Ensembles of Nitrogen-Vacancy Centers in Diamond, *Nano Lett.* **18**, 4046 (2018).
- [22] A. Jarmola, V. M. Acosta, K. Jensen, S. Chemerisov, and D. Budker, Temperature- and magnetic-field-dependent longitudinal spin relaxation in nitrogen-vacancy ensembles in diamond, *Phys. Rev. Lett.* **108**, 197601 (2012).
- [23] M. Mrózek, D. Rudnicki, P. Kehayias, A. Jarmola, D. Budker, and W. Gawlik, Longitudinal spin relaxation in nitrogen-vacancy ensembles in diamond, *EPJ Quantum Technol.* **2** (2015).
- [24] A. Norambuena, E. Muñoz, H. T. Dinani, A. Jarmola, P. Maletinsky, D. Budker, and J. R. Maze, Spin-lattice relaxation of individual solid-state spins, *Phys. Rev. B* **97**, 094304 (2018).
- [25] S. T. Alsid, J. F. Barry, L. M. Pham, J. M. Schloss, M. F. O’Keeffe, P. Cappellaro, and D. A. Braje, Photoluminescence Decomposition Analysis: A Technique to Characterize N - V Creation in Diamond, *Phys. Rev. Applied* **12**, 044003 (2019).
- [26] O. R. Opaluch, N. Oshnik, R. Nelz, and E. Neu, Optimized Planar Microwave Antenna for Nitrogen Vacancy Center Based Sensing Applications, *Nanomaterials* **11** (2021).
- [27] V. M. Acosta, E. Bauch, M. P. Ledbetter, A. Waxman, L.-S. Bouchard, and D. Budker, Temperature dependence of the nitrogen-vacancy magnetic resonance in diamond, *Phys. Rev. Lett.* **104**, 070801 (2010).
- [28] K.-M. C. Fu, C. Santori, P. E. Barclay, L. J. Rogers, N. B. Manson, and R. G. Beausoleil, Observation of the dynamic Jahn-Teller effect in the excited states of nitrogen-vacancy centers in diamond, *Phys. Rev. Lett.* **103**, 256404 (2009).
- [29] X.-D. Chen, C.-H. Dong, F.-W. Sun, C.-L. Zou, J.-M. Cui, Z.-F. Han, and G.-C. Guo, Temperature dependent energy level shifts of nitrogen-vacancy centers in diamond, *Appl. Phys. Lett.* **99**, 161903 (2011).
- [30] M. W. Doherty, V. M. Acosta, A. Jarmola, M. S. J. Barson, N. B. Manson, D. Budker, and L. C. L. Hollenberg, Temperature shifts of the resonances of the NV– center in diamond, *Phys. Rev. B* **90**, 041201(R) (2014).
- [31] Y. Y. Hui, O. Y. Chen, T. Azuma, B.-M. Chang, F.-J. Hsieh, and H.-C. Chang, All-Optical Thermometry with Nitrogen-Vacancy Centers in Nanodiamond-Embedded Polymer Films, *J. Phys. Chem. C* **123**, 15366 (2019).
- [32] T.-I. Yang, T. Azuma, Y.-W. Huang, Y. Y. Hui, C.-T. Chiang, and H.-C. Chang, Stimulated emission cross sections and temperature-dependent spectral shifts of neutral nitrogen-vacancy centers in diamonds, *J. Chin. Chem. Soc.* **70**, 451 (2023).
- [33] T. Wolf, P. Neumann, K. Nakamura, H. Sumiya, T. Ohshima, J. Isoya, and J. Wrachtrup, Subpicotesla Diamond Magnetometry, *Phys. Rev. X* **5**, 041001 (2015).
- [34] S. Ernst, P. J. Scheidegger, S. Diesch, L. Lorenzelli, and C. L. Degen, Temperature Dependence of Photoluminescence Intensity and Spin Contrast in Nitrogen-Vacancy Centers, *Phys. Rev. Lett.* **131**, 086903 (2023).
- [35] N. Nunn, S. Milikisijants, M. D. Torelli, R. Monge, T. Delord, A. I. Shames, C. A. Meriles, A. Ajoy, A. I. Smirnov, and O. A. Shenderova, Optical and electronic spin properties of fluorescent micro- and nanodiamonds upon prolonged ultrahigh-temperature annealing, *J. Vac. Sci. Technol. B* **41**, 042206 (2023).
- [36] M. Capelli, L. Lindner, T. Luo, J. Jeske, H. Abe, S. Onoda, T. Ohshima, B. Johnson, D. A. Simpson, A. Stacey, P. Reineck, B. C. Gibson, and A. D. Greentree, Proximal nitrogen reduces the fluorescence quantum yield of nitrogen-vacancy centres in diamond, *New J. Phys.* **24**, 033053 (2022).
- [37] A. Bhaumik, R. Sachan, and J. Narayan, Tunable charge states of nitrogen-vacancy centers in diamond for ultrafast quantum devices, *Carbon* **142**, 662 (2019).
- [38] R. Guo, K. Wang, Y. Zhang, Z. Xiao, G. Jia, H. Wang, Y. Wu, and Y. Tian, Adjustable charge states of nitrogen-vacancy centers in low-nitrogen diamond after electron

irradiation and subsequent annealing, *Appl. Phys. Lett.*

117, 172104 (2020).